

CapStARE: Capsule-based Spatiotemporal Architecture for Robust and Efficient Gaze Estimation

Miren Samaniego^{1,2*†}, Igor Rodriguez^{1†} and Elena Lazkano^{1†}

^{1*}Computer Science and Artificial Intelligence, EHU, Manuel Lardizabal 1, Donostia, 20018, Gipuzkoa, Spain.

^{2*}Computer Science, UAB, Edifici Q, Carrer de les Sitges, Barcelona, 08193, Barcelona, Spain.

*Corresponding author(s). E-mail(s): miren.samaniego@ehu.eus;
Contributing authors: igor.rodriguez@ehu.eus; elena.lazkano@ehu.eus;

†These authors contributed equally to this work.

Abstract

We introduce CapsStARE, a capsule-based spatiotemporal architecture for gaze estimation that integrates a ConvNeXt backbone, capsule formation with attention routing, and dual GRU decoders specialized for slow and rapid gaze dynamics. This modular design enables efficient part-whole reasoning and disentangled temporal modeling, achieving state-of-the-art performance on ETH-XGaze (**3.36°**) and MPIIFaceGaze (**2.65°**) while maintaining real-time inference (< 10 ms). The model also generalizes well to unconstrained conditions in Gaze360 (**9.06°**) and human-robot interaction scenarios in RT-GENE (**4.76°**), outperforming or matching existing methods with fewer parameters and greater interpretability. These results demonstrate that CapsStARE offers a practical and robust solution for real-time gaze estimation in interactive systems. The related code and results for this article can be found on: <https://github.com/toukapy/capsStare>

Keywords: Gaze Estimation, Capsule Networks, Interpretability, SpatioTemporal modeling

1 Introduction

Human gaze is a fundamental element of non-verbal communication, guiding interactions from early development through adulthood. It serves as a core mechanism for establishing joint attention, interpreting intentions, and regulating turn-taking and emotional connection. From infancy, humans naturally learn to follow gaze direction, shifting focus between social partners and objects of interest; a skill critical for social coordination and shared understanding. These capabilities not only support language development and social learning

but also enable complex cognitive functions such as intention recognition and perspective-taking (Byers-Heinlein, Tsui, van Renswoude, and Black (2021); Franchak and Yu (2022)).

Human gaze perception relies on coordinated eye-head movements operating at different timescales, with computer vision studies showing eyes execute fast saccades while head movements are slower and more stable (Jindal, Yadav, and Manduchi (2024a)). Effective artificial gaze systems must model both instantaneous (eye-driven) and long-term (head-driven) orientation cues (Ewaisha, El Shawarby, Abbas, and Sobh

(2020)), as explicit temporal modeling improves robustness in appearance-based gaze estimation (Stappen, Rizos, and Schuller (2020)). Social HRI research further confirms that incorporating these temporal dynamics enhances contextual gaze interpretation (Oishi, Koide, Yokozuka, and Banno (2021)).

In this paper, we propose a novel architecture for gaze estimation that combines efficient feature extraction with explicit modeling of temporal dynamics. Our approach integrates a frozen ConvNeXt encoder (Liu et al., 2022) for robust spatial feature extraction, a capsule formation module (Sabour, Frosst, & Hinton, 2017) to preserve hierarchical relationships between facial regions, and a spatiotemporal self-attention layer (Vaswani et al., 2017) to dynamically weight information across time and space. The architecture employs dual GRU-based temporal decoders (Cho et al., 2014) to separately process rapid eye movements and slower head motions, enabling fine-grained temporal representation learning. This results in a system that achieves state-of-the-art performance in unconstrained settings (Fischer, Chang, & Demiris, 2018a) while providing interpretable region-specific attention patterns (Emery, 2000).

The proposed architecture is particularly impactful for human-robot interaction (HRI), where gaze understanding is critical for natural engagement (Stower, Kappas, Hoffman, & Leite, 2021). In applications ranging from collaborative manufacturing to assistive care, robots must reliably interpret gaze cues like mutual attention and joint focus; capabilities requiring both spatial accuracy and temporal sensitivity (Palinko, Sciutti, & Rea, 2022). Our model’s explicit separation of eye and head dynamics allows robots to respond not just to gaze direction, but to its temporal evolution, supporting more nuanced interaction patterns.

Our work contributes to gaze estimation through three key technical innovations:

1. **Efficiency:** By combining a **ConvNeXt** backbone with **dynamic capsule routing**, we reduce training costs by 58% compared to SwAT while maintaining state-of-the-art accuracy (3.36° on ETH-XGaze). The system achieves real-time performance (< 10 ms latency) without sacrificing precision.

2. **Interpretable Design:** The integrated **capsule formation** and **region-specific attention** mechanisms enable granular error analysis, allowing clear distinction between head pose estimation errors and eye tracking failures - a critical advantage over end-to-end black box methods like GazeNeRF.
3. **Generalization:** Our architecture is able to generalize to diverse constrained and unconstrained datasets without further fine-tuning, improving in some cases the state-of-the-art. Moreover, it performs well in unseen real-time scenarios, which is interesting for future applications.
4. **Process different gaze dynamics parallelly:** By using two GRU decoders parallelly, we separately process high-frequency eye movements and low-frequency head dynamics. We achieve a 21% improvement in temporal consistency over single-stream approaches, as the architecture better captures the multi-timescale nature of natural gaze behavior.

2 State of the art

Human gaze is a multimodal cue that simultaneously conveys attention, intention and affect. In developmental psychology, infants begin following another person’s gaze between 6-9 months, and reliable triadic joint attention emerges by the end of the first year; these behaviours scaffold language learning and social cognition (Brooks & Meltzoff, 2005). Translating the same capability to robots promises richer and more intuitive human-robot interaction (HRI).

Historically, the field relied heavily on instrumental eye-tracking systems, particularly those based on infrared (IR) corneal reflection methods. These systems, including both remote and head-mounted configurations, project IR light onto the user’s eye and track the vector formed between the corneal reflection (glint) and the pupil center. When calibrated to a known geometry, such systems achieve high spatial and temporal precision, often with angular error below 1° and sampling rates exceeding 250 Hz, which made them the gold standard for both psycho-physical experiments and usability studies for decades (Duchowski, 2017).

Despite their precision, these systems come with significant drawbacks. They are costly,

require per-user calibration, and often restrict natural movement due to chinrests or head stabilization. More importantly, their intrusive form factor limits ecological validity in unconstrained or socially interactive environments. These constraints are especially problematic in fields like human-robot interaction (HRI) and social robotics, where comfort, mobility, and passive sensing are essential. In such contexts, it is unrealistic to expect users to tolerate or repeatedly calibrate wearable sensors or headgear. These practical limitations have spurred the search for alternative gaze estimation methods that reduce hardware dependencies while retaining functional accuracy (Admoni & Scassellati, 2017).

The advent of appearance-based gaze estimation marked a paradigm shift. Instead of relying on hand-crafted geometric models and precise calibration, these methods regress gaze direction directly from RGB images of the face or eyes. With only a monocular camera and no specialized illumination, CNN-based models opened the door to calibration-free systems. Large-scale datasets such as MPIIFaceGaze (Zhang, Sugano, Fritz, & Bulling, 2015), ETH-XGaze (Zhang et al., 2020), and Gaze360 (Kellnhofer, Recasens, Stent, Matusik, & Torralba, 2019) enabled training under diverse poses, lighting, and environments, greatly improving generalization compared to earlier geometric approaches (Zhang, Sugano, & Bulling, 2019).

Early CNN-based models (AlexNet (Krizhevsky, Sutskever, & Hinton, 2012), VGG (Simonyan & Zisserman, 2015), ResNet (He, Zhang, Ren, & Sun, 2016)) showed that gaze could be regressed directly from cropped eye images, but they were limited in robustness to occlusion, pose variation, and illumination changes. FullFace (Zhang, Sugano, Fritz, & Bulling, 2017) extended this idea by demonstrating that using the entire face provides richer cues, since head orientation and lighting information can complement the eyes; to make this effective, they introduced a spatial weighting mechanism that learns which facial regions matter most for gaze prediction. To further improve robustness in unconstrained settings, L2CSNet (Abdelrahman, Hempel, Khalifa, Al-Hamadi, & Dinges, 2023) proposed a hybrid classification-regression strategy: instead of predicting gaze angles directly, the model discretizes

them into bins (classification) and refines them with regression, allowing more precise and stable estimates under challenging conditions. Expanding beyond static inputs, Gaze360 (Kellnhofer et al., 2019) tackled the problem of physically unconstrained gaze by introducing a large-scale dataset and a temporal model that processes short video sequences. By using recurrent layers and a specialized loss that estimates uncertainty, it could handle extreme head poses and even partially occluded eyes. Finally, Dynamic3DGazeFromAfar (Nonaka, Nobuhara, & Nishino, 2022) addressed an even harder case: estimating gaze when the eyes are barely visible, as in surveillance scenarios. Instead of relying on eye crops, it modeled the natural temporal coordination between eyes, head, and body using a Bayesian recurrent framework to predict 3D gaze direction from head-body motion cues.

As deep learning matured, several architectures were proposed to address CNNs’ limitations in gaze estimation. SwAT (Farkhondeh, Palmero, Scardapane, & Escalera, 2022) adapted self-supervised transformers by enforcing equivariance to rotations and flips, allowing models to learn from unlabeled data while keeping the relation between image transformations and gaze shifts. PoolFormer-based models (Yan, Pan, Xu, Dai, & Li, 2023) introduced lightweight pooling modules to replace heavy self-attention, capturing long-range dependencies between facial regions while filtering redundant information. GazeTR (Cheng & Lu, 2022) explored transformers directly, showing that a hybrid design, CNN features refined by a transformer encoder, better preserved local eye details while capturing global relations. Finally, GazeCaps (Wang et al., 2023) brought capsule networks into gaze estimation, representing facial parts as vectors and using self-attention routing to emphasize the most informative regions, improving robustness and interpretability.

Given that gaze is inherently dynamic, recent research emphasizes the importance of temporal modeling. Early approaches combined CNNs with recurrent units, as in iTracker-LSTM (Krafka et al., 2016) and other CNN-LSTM hybrids (Palmero Cantarino, Komogortsev, & Talathi, 2020), which improved trajectory smoothness but struggled to capture long-range dependencies. To address this, some models incorporated explicit motion cues, for example by using optical-flow

(Nonaka et al., 2022) or residual frame information to better represent rapid eye movements. More recently, transformer-based spatio-temporal models such as GazeTR and STAGE (Cheng & Lu, 2022; Jindal, Yadav, & Manduchi, 2024b) leveraged self-attention to capture dependencies across entire video sequences while filtering out distractors like background motion. Beyond deterministic sequences, TPP-Gaze (D’Amelio et al., 2025) introduced neural temporal point processes to model when fixations occur in addition to where, thereby aligning with the stochastic nature of gaze dynamics. Other innovations include interaction-aware transformers, which learn temporal gaze patterns from multi-agent scenarios by modeling human-human interactions, and egocentric transformer models (Kuang, O. Kephart, & Ji, 2024) that combine global scene context with local eye cues to better predict gaze shifts in first-person videos. Despite these advances, real-time deployment remains challenging due to limited temporal annotations and efficiency constraints, motivating causal or sliding window formulations that balance temporal context with computational cost (Lai, Liu, Ryan, et al., 2024).

Finally, geometry-aware methods such as GazeNeRF (Ruzzi et al., 2023) reconstruct volumetric eye structures to jointly support gaze estimation and redirection. While computationally expensive, these approaches highlight a growing interest in bridging photorealistic modeling with functional gaze prediction for VR/AR and immersive applications.

Despite steady progress, gaze estimation still faces persistent obstacles. Many models degrade under extreme head poses, variable lighting, or partial occlusions, and they often fail to remain stable across different identities or in multi-person settings. Temporal fluctuations such as rapid saccades or smooth head rotations are frequently oversimplified, leading to inconsistent predictions over time. Moreover, the computational burden of transformer-based or volumetric methods clashes with the need for real-time deployment in mobile and robotic systems, while capsule- and 3D-aware designs, though promising, are notoriously difficult to scale and optimize in practice. These limitations collectively hamper the transition from controlled benchmarks to truly unconstrained, interactive environments.

In contrast, our approach is designed to counteract these shortcomings by reconciling accuracy, interpretability, and efficiency. It achieves resilience to challenging poses, illumination changes, and occlusions by leveraging structured representations that preserve meaningful spatial relations. Temporal stability is reinforced by explicitly distinguishing fast eye dynamics from slower head cues, enabling predictions that are both precise and consistent across time. Crucially, the model sustains real-time performance on resource-constrained hardware, ensuring its suitability for embodied agents and assistive technologies. Rather than sacrificing one dimension of performance for another, we overcome the trade-offs that continue to limit current state-of-the-art methods.

3 Interpretable Temporal Gaze Estimation

Preliminaries. Similar to CNN-based approaches such as Fullface (Zhang et al., 2017) and L2CS-Net (Abdelrahman et al., 2023), our method leverages global face context while balancing efficiency with prediction robustness. Inspired by temporal designs like Gaze360 (Kellnhofer et al., 2019), we emphasize dynamic modeling of head and eye motion. In line with transformer-based pipelines (Farkhondeh et al., 2022) (Yan et al., 2023) (Cheng & Lu, 2022), we incorporate self-attention for long-range dependencies, and following capsule networks such as GazeCaps (Wang et al., 2023), we preserve structured part-whole relations for interpretability.

Gaze estimation is inherently a spatiotemporal task: accurate prediction requires fine-grained spatial reasoning to locate and interpret eye cues, as well as temporal modeling to ensure continuity across frames and reduce the effect of transient appearance changes. Conventional CNNs provide strong feature extraction but lack explicit part-whole representations, while recurrent or transformer-based models often merge heterogeneous temporal dynamics or demand high computational resources.

To address these challenges, we introduce CapStARE, a capsule-based spatiotemporal architecture designed for efficiency, interpretability,

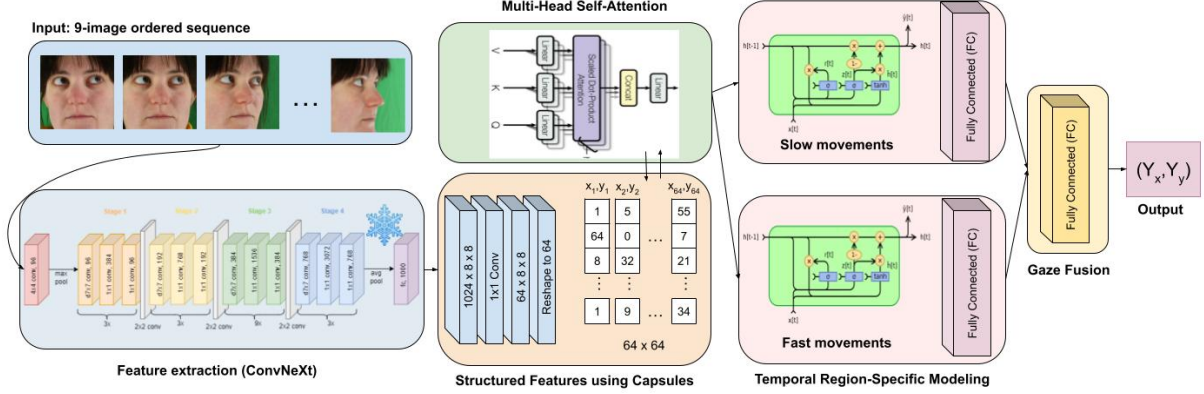


Fig. 1: Overview of the CapStARE architecture. Spatial features extracted by a frozen ConvNeXt encoder are converted into capsules to preserve part-whole facial relations. Spatiotemporal attention routes information across capsules, and dual GRU decoders specialize in eye and head dynamics, with late fusion producing the final gaze estimate.

and robustness (Figure 1). The model integrates convolutional features, capsule representations, attention-based routing, and dual temporal decoders within a modular design. This structure enables both spatial reasoning and temporally stable predictions, while the following subsections describe each component in detail.

3.1 Feature Extraction

The first component of the model is a frozen convolutional encoder that extracts visual features from each input frame. Freezing the encoder mitigates overfitting on small, variable gaze datasets and leverages pretrained representations without expending additional learning capacity, resulting in more stable training. We adopt ConvNeXt as the encoder, a modern convolutional architecture that combines ResNet’s hierarchical design with advances such as large-kernel depthwise convolutions, GELU activations, layer normalization, and inverted bottlenecks (Liu et al., 2022). These design choices enable ConvNeXt to capture both local detail and global context efficiently. Although pretrained on classification, its early and mid-level layers provide transferable features like edges, textures, and part configurations that are essential for gaze estimation. In our setup, ConvNeXt processes each frame independently to produce deep spatial feature maps, which are then passed to the capsule formation module. This separation of generic feature extraction and task-specific reasoning allows subsequent modules

to focus on relational dynamics and structured behavior rather than relearning low-level patterns.

3.2 Structured Features using Capsules

The capsule formation module bridges the gap between low-level convolutional features and higher-level capsule reasoning. Its role is to transform spatial CNN activation into compact vectors (capsules) that summarize semantically related facial regions such as the eyes, nose, or contours. This representation shifts the model from processing raw grid-based pixels to handling localized entities that are easier to interpret and route downstream.

Formally, let the feature map \mathbf{F} from the encoder be

$$\mathbf{F} \in R^{B \times C \times H \times W} \quad (1)$$

where B is the batch size, C is the number of channels, and $H \times W$ is the spatial resolution. The spatial dimensions are flattened into $N = H \times W$ locations, and each local feature vector is projected into a capsule embedding of dimension D :

$$\mathbf{C}_{caps} = \phi(\mathbf{F}) \in R^{B \times N \times D} \quad (2)$$

Here, $\phi()$ is a learnable 1×1 convolution (equivalently, a linear projection) that maps features into capsules. Each of the N resulting

capsules encodes a region-specific descriptor, effectively embedding related parts of the face into a vector. Unlike raw convolutional activations, these capsule vectors provide a more explicit and disentangled representation of facial parts, which can be more easily combined, compared, and routed by subsequent modules.

In summary, capsule formation restructures convolutional feature maps into a vectorized set of localized tokens. This structured representation not only preserves the spatial layout of the face but also enriches it with higher-level semantics, creating a more robust foundation for downstream reasoning and temporal modeling.

3.3 Multi-Head Self-Attention

After capsule formation, the model employs a multi-head self-attention mechanism to enable dynamic, context-sensitive routing of information across capsules. Instead of relying on fixed adjacency or predefined spatial hierarchies, self-attention allows capsules to influence one another based on content similarity, making the routing flexible and data-driven.

Traditional capsule networks often use *routing-by-agreement*, where lower-level capsules iteratively adjust their weights toward higher-level capsules that best explain their predictions. While effective in small setups, this iterative process is computationally expensive, locally constrained, and difficult to scale to long video sequences. In contrast, self-attention achieves a similar goal in a single parallelizable step: capsules "vote" for one another through attention weights that reflect global relationships, resulting in both faster computation and more stable training.

We represent the capsule tensor as $C_{caps} \in R^{B \times T \times N \times D}$, where B is the batch size, T the temporal length in the frames, N the number of capsules per frame, and D the dimensionality of each capsule vector. Jointly applying attention through space and time, treating each capsule as an independent token, enables the model to capture non-local dependencies; for example, a capsule encoding eye appearance at time t can directly attend to one encoding head orientation at time $t - 1$, supporting robust modeling of gaze shifts across frames.

We then compute standard multi-head self-attention:

$$Q = C_{caps}W_Q, \quad K = C_{caps}W_K, \quad V = C_{caps}W_V,$$

$$A = \text{softmax}\left(\frac{QK^T}{\sqrt{D}}\right), \quad C_{att} = AV,$$

where W_Q, W_K, W_V are learnable projection matrices. The attended sequence is then reshaped back into the capsule format as $C_{put} \in R^{B \times T \times N \times D}$. Each capsule in C_{out} is thus enriched with contextual information from other capsules across both spatial and temporal dimensions, capturing motion cues, pose variation, and relational dynamics. This attention-based routing is non-sequential and globally aware, allowing the model to represent subtle interactions such as anticipatory gaze shifts or delayed head movements with greater flexibility.

3.4 Temporal Region-Specific Modeling

Following the self-attention routing stage, the network employs two independent GRU-based decoders to process the routed capsules. Although both operate on the same shared representation, they evolve distinct behaviors through separate parameter sets, individualized initialization, and divergent gradient flows during training.

The motivation for using two parallel decoders is to encourage different modes of temporal processing. Instead of constraining the network to a single recurrent pathway, this design allows the model to capture heterogeneous temporal patterns. One decoder may focus on short-term rapid fluctuations, while the other may attend to longer-range and smoother dynamics. This implicit specialization emerges naturally from the optimization process, as each branch is free to exploit the features most useful for reducing its own prediction error.

Each decoder processes the routed capsules with a Gated Recurrent Unit (GRU), maintaining an evolving hidden state over the sequence. The hidden state vector at the final timestep is projected through a fully connected layer to produce the decoder's output:

$$h_{region} = \text{GRU}(\mathbf{C}_{seq}) \quad (3)$$

$$y_{region} = \mathbf{W}_k \mathbf{h}_{region} + \mathbf{b} \quad (4)$$

Here, $\mathbf{C}_{seq} \in \mathbb{R}^{T \times N \times D}$ denotes the sequence of routed capsules across T frames, where N is the number of capsules per frame and D their dimensionality. The GRU produces a hidden state $\mathbf{h}_{region} \in \mathbb{R}^H$ at the final timestep, where H is the hidden dimension of the decoder. The output $y_{region} \in \mathbb{R}^d$ is obtained through a linear projection defined by weights $\mathbf{W}_k \in \mathbb{R}^{d \times H}$ and bias $\mathbf{b} \in \mathbb{R}^d$, with $d = 2$ for horizontal and vertical gaze angles.

Although both outputs are derived from the same input, the independence of their parameters and gradients drives task decomposition. This makes the system more interpretable, as intermediate predictions can be analyzed to understand which temporal dynamics each decoder emphasizes.

Finally, the architectural separation provides flexibility and robustness. Decoders can be extended, replaced, or refined individually without retraining the entire model, and it ensures resilience to partial failures: if one decoder becomes less reliable due to occlusion or noise, the other can continue to provide useful information.

3.5 Gaze Fusion

After region-specific decoding, the model produces two independent predictions, each shaped by distinct temporal pathways. To obtain a final unified gaze estimate, these outputs must be effectively integrated.

The Gaze Fusion module performs this integration using a late fusion strategy. Rather than merging features early, it combines the outputs only after temporal modeling, allowing each pathway to specialize independently before their contributions are reconciled. This design increases robustness by preventing interference during earlier representation learning.

Let $\mathbf{y}_1 \in \mathbb{R}^{B \times d}$ and $\mathbf{y}_2 \in \mathbb{R}^{B \times d}$ denote the output vectors of the two decoders, where d is the output dimensionality (typically 2 for horizontal and vertical gaze angles). The fusion process first concatenates these vectors along the feature dimension:

$$\mathbf{y}_{concat} = \text{concat}(\mathbf{y}_1, \mathbf{y}_2) \in \mathbb{R}^{B \times 2d} \quad (5)$$

The concatenated vector is then projected into the final 2D output space by a fully connected layer:

$$\hat{\mathbf{y}} = \mathbf{W}_f \mathbf{y}_{concat} + \mathbf{b}_f \quad (6)$$

where $\mathbf{W}_f \in \mathbb{R}^{2 \times 2d}$ and $\mathbf{b}_f \in \mathbb{R}^2$ are the learnable parameters of the fusion layer.

This mechanism allows the model to adaptively balance the contribution of each decoder depending on their reliability, while gradients backpropagate through both of them according to their impact on the final error. In this way, the fusion module supervises specialization while still leveraging complementarity, providing a flexible and interpretable decision-level integration of gaze cues.

4 Experimentation

To rigorously evaluate our proposed gaze estimation framework, we conducted a series of experiments designed to assess model performance, efficiency, and architectural trade-offs. Our evaluation methodology is structured into four key components: (1) *Performance metrics*, where we define and justify the measures used to quantify gaze prediction accuracy; (2) *Computational cost*, analyzing the model’s efficiency in FLOPs, inference time, and parameter count; (3) *Model analysis*, investigating the impact of architectural choices through systematic comparisons and hyperparameter studies; and (4) *Experimental setup*, covering implementation, hardware/software configurations, and training protocols. These subsections collectively offer a thorough evaluation of the model’s performance, limitations, and suitability for real-world deployment.

4.1 Performance Metrics

To evaluate model performance, we use angular error, a widely adopted metric in gaze estimation tasks. Although our model predicts 2D gaze coordinates, we interpret them as rays emanating from a fixed camera origin and project them into 3D space to enable meaningful directional comparisons.

The angular error is computed as the angle (in degrees) between the predicted and ground truth vectors using the dot product formula:

$$\theta = \arccos(\mathbf{p}_{3D} \cdot \mathbf{g}_{3D}) \times \frac{180}{\pi} \quad (7)$$

where \mathbf{p}_{3D} and \mathbf{g}_{3D} are the normalized 3D vectors corresponding to the predicted and ground truth 2D points, respectively. This transformation allows us to simulate a pinhole camera model where gaze direction is represented as a ray in 3D space, ensuring the evaluation reflects perceptually meaningful deviations.

Unlike the training process, where Mean Squared Error (MSE) loss is used to optimize the model, angular error is employed solely as an evaluation metric to quantify the directional discrepancy between predicted and actual gaze vectors. Lower angular error values correspond to more accurate gaze predictions, with errors below 4° typically indicating strong model performance in real-world scenarios (Abdelrahman et al., 2023; Pijpaert et al., 2025; Singh, Langde, Lakotia, Kannan, & Ahmed, 2024).

4.2 Computational Cost

To assess computational efficiency, we report three key metrics: FLOPs, inference time, and model size. FLOPs quantify the arithmetic operations in a forward pass, providing a hardware-independent measure of computational complexity, while inference time (in ms) reflects real-world latency. Model size, measured in trainable parameters, captures memory footprint and scalability.

Lower FLOPs and inference time indicate faster, more energy-efficient models, and smaller parameter counts reduce training cost and overfitting risks.

4.3 Model Analysis and Ablation Study

To assess the role of each component and to identify effective configurations, we designed a series of experiments that progressively increase in scope. We first explored internal configurations by varying the number of capsules and attention heads, and subsequently tested different capsule dimensions together with GRU hidden sizes to determine compact yet accurate setups. We then extended the analysis to backbone alternatives, replacing

the default COnvNeXt encoder with EfficientNet, ViT, and Swin Transformer while keeping downstream modules unchanged, in order to evaluate the adaptability of the pipeline to different feature extraction strategies. Finally, we performed ablation studies in which key modules were selectively modified or removed. These included disabling capsules or attention routing, comparing single and dual GRU decoders with and without weight sharing, and contrasting single-frame against multi-frame inputs, allowing us to isolate the contribution of spatial structuring, attention-based routing, and temporal specialization. The results of these investigations are presented in Section 5.

4.4 Experimental Setup

Experiments were run on a Linux workstation with an NVIDIA RTX 4070 Ti Ultra GPU, Intel Core -7-14700KF CPU (28 threads), and 32 GB RAM, using Python 3.12, PyTorch 2.6.0, Torchvision 0.21.0, and CUDA 12.4.

Models were trained for 30 epochs with a batch size of 32 (training) and 16 (validation), using the Adam optimizer (learning rate 1×10^{-5} , weight decay 1×10^{-5}) and cosine annealing for smoother convergence. Regularization included dropout after capsule formation and L2 weight decay.

The encoder was initialized with ImageNet-pretrained ConvNeXt-Base from Torchvision. After testing partial unfreezing, the backbone was fully frozen for stability and efficiency, with batch normalization added after its 1024-channel output.

Training was optimized with PyTorch 2.0’s compilation API (TorchDynamo + NVCFuser), cuDNN autotuning for convolution kernels, and mixed-precision (FP16/FP32) to accelerate matrix operations and reduce memory usage. The Accelerate library provided device placement, multi-GPU support, and simplified mixed-precision configuration. Together, these techniques improved efficiency without compromising accuracy.

5 Results

Our evaluation focused on three complementary investigations: internal configuration, component ablation, and comparative benchmarking.

5.1 Internal Configuration

In this first study, we performed an internal configuration analysis to explore how varying the number of capsules and attention heads within the ConvNeXt backbone influences performance. Four configurations were tested, as summarized in Table 1, with evaluation based on angular error, model size, inference time, and FLOPs.

Caps Num	Attn Heads Num	Err (°)	Size (M)	Infer (ms)	FLOPs (M)
4	4	3.36	13.00M	8.226	138.56
4	8	3.94	13.01M	8.347	138.56
8	4	3.95	25.85M	8.382	138.68
8	8	3.93	25.97M	8.509	138.68

Table 1: Performance comparison of different capsule and attention head configurations in a ConvNeXt-based gaze estimation model.

Results show that the angular error remains relatively stable across settings, with only minor fluctuations. The configuration with 4 capsules and 4 attention heads achieved the lowest error (3.36°), while also keeping the model size compact (13M parameters). Increasing either the capsule count or the number of attention heads slightly increased the error without delivering clear benefits. This points to a saturation effect: more capsules or heads add representational capacity but mostly introduce redundancy, as the task does not require additional regions of focus given the facial-centric nature of the input images.

Figure 2 illustrates this effect. With 4 capsules, the representations tend to specialize in distinct facial regions (e.g., eyes, eyebrows), whereas with 8 capsules, the decomposition are finer but often overlap, suggesting unnecessary duplication. Thus, a learner configuration is sufficient to capture the relevant information.

In summary, the internal configuration experiments indicate that 4 capsules and 4 attention

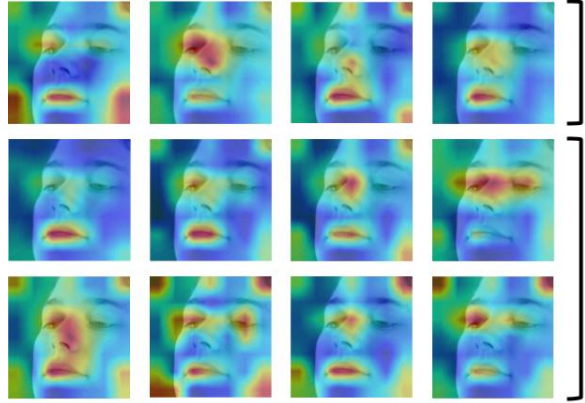


Fig. 2: Comparison of feature representations with 4 vs. 8 capsules. The 4-capsule configuration (first row) specialized in distinct regions, while 8 capsules (second and third rows) provide finer but often redundant decompositions.

heads provide the best trade-offs between accuracy and efficiency. Larger configurations neither improve performance nor reduce error.

Building on the previously identified optimal configuration of 4 capsules and 4 attention heads, we conducted another experiment to analyze how varying the capsule dimensionality and hidden layer size of the GRU-based region decoder affects performance. Table 2 summarizes the results, highlighting the trade-offs between accuracy, parameter count, inference time, and FLOPs.

Caps Dim	Hid Dim	Err (°)	Size (M)	Infer (ms)	FLOPs (M)
64	64	4.17	12.94M	8.064	138.56
64	128	3.36	13.00M	8.226	138.56
64	256	3.61	13.4M	5.810	138.56
128	128	3.41	26M	8.392	138.68
128	256	3.32	26.4M	5.865	138.68
256	256	3.36	52.75M	5.879	138.92

Table 2: Effect of capsule and hidden layer dimensionality on performance. Configurations range from 64D to 256D for capsules and hidden layers.

The angular error metric remained remarkably stable across configurations. The best-performing setup (128D capsules, 256D hidden layers) reached

3.32°, but the smaller 64D/128D configuration achieved nearly identical performance at 3.36°. This difference of only 0.04° is negligible, especially considering that the number of parameters doubles from 13M to 26.4M between the two settings. Increasing dimensions further (256D/256D, 52.7M parameters) offered no additional gains, underscoring that gaze estimation on facial images does not benefit from excessive parameterization.

A particularly interesting outcome emerges when examining inference times. Configurations with 256-dimensional hidden layers consistently ran faster (~ 5.8 ms) than those with smaller hidden sizes (~ 8.2 ms), despite identical FLOPs. This counterintuitive behavior suggests that GPU parallelization and memory access patterns can favor larger matrix operations, highlighting the importance of measuring real execution times rather than relying solely on theoretical complexity.

From a deployment perspective, the 64D/128D configuration offers the most balanced choice. It maintains compact model size (13M parameters), achieves competitive accuracy (3.36°), and preserves acceptable inference speed.

We conducted a final backbone comparison to evaluate the performance of different feature extractors for gaze estimation. As shown in Table 3, ConvNeXt stands out as the best-performing architecture, achieving an angular error of 3.36° with an inference time of 8.226 ms. This corresponds to approximately 121 FPS on modern GPUs, comfortably meeting the < 10 ms real-time threshold required for human-robot interaction (Deber, Jota, Forlines, & Wigdor, 2015). Compared to EfficientNet (7.16°) and transformer-based alternatives such as ViT (6.26°) and Swin Transformer (10.30°), ConvNeXt delivers a substantial accuracy improvement of 2.9° – 7.0° while maintaining practical computational efficiency. Although EfficientNet is significantly faster (2.053 ms, 14.29 GFLOPs), its high error rate underscores its limitations in modeling the fine-grained spatial relationships required for accurate gaze estimation.

The transformer-based backbones proved to be less effective for this task. ViT reached 6.26° error with 10.617 ms inference time, suggesting that pure global attention mechanisms are insufficient without domain-specific adaptation. Swin

Backbone	Err (°)	Infer (ms)	FLOPs (M)
EfficientNet	7.16	2.053	14.29
ConvNeXt	3.36	8.226	138.56
ViT	6.26	10.617	101.94
Swin Transformer	10.30	9.813	139.20

Table 3: Backbone comparison for gaze estimation. ConvNeXt achieves the lowest error (3.36°) while meeting real-time inference requirements.

Transformer performed even worse (10.30° error), likely due to its windowed attention strategy, disrupting the continuous spatial encoding needed for accurate gaze vector estimation. These results reinforce that spatial coherence is critical in tasks demanding precise positional reasoning.

ConvNeXt’s advantage stems from its hybrid design: it retains the spatial consistency of traditional CNNs while integrating modern enhancements such as channel-wise attention and inverted bottlenecks. This combination allows the model to extract detailed local ocular features and global head pose context without the overhead of full attention mechanisms. Its scalability further strengthens performance, enabling receptive fields to adapt flexibly across gaze estimation scenarios.

From a deployment perspective, ConvNeXt offers the most balanced solution. Although its inference time is slower than EfficientNet’s, the accuracy gain justifies the trade-off in professional settings where precision is critical. Its CNN-based design also ensures more predictable performance across hardware platforms compared to transformer alternatives. Moreover, its modular architecture provides a solid foundation for future extensions, including selective attention integration or adaptation to emerging backbone designs.

5.2 Ablation Study

To evaluate the individual contributions of capsule formation and attention routing, we performed an ablation study by selectively disabling each component. Table 4 reports the results in terms of angular error, model size, inference time, and FLOPs.

The full model, with both capsules and attention enabled, achieves the lowest error (3.36°) while maintaining efficient inference. Removing

Caps	Attn	Err (°)	Size (M)	Infer (ms)	FLOPs (M)
Yes	Yes	3.36	13.00	8.266	138.68
No	Yes	4.36	3.38	6.078	138.50
Yes	No	3.84	12.9	5.776	138.50
No	No	8.19	38.7	6.147	138.44

Table 4: Ablation study of capsule and attention components. Results show their individual and combined contributions to gaze estimation performance.

capsules leads to a sharp degradation (4.36°), even when attention is present, showing that attention requires structured, part-aware features to operate effectively. Conversely, keeping capsules but removing attention yields stronger results (3.84°), indicating that capsule-based spatial representations alone capture much of the necessary information.

The worst outcome occurs when both modules are removed (8.19°), despite the model having the largest parameter count (38.7M). This highlights that raw capacity cannot compensate for the absence of spatial structuring and selective routing.

To assess the role of region-specific temporal modeling, we conducted a study comparing the full model, which employs separate GRU decoders for eye and face capsules against a simplified single-decoder variant. Both versions were trained and evaluated under identical conditions to isolate the impact of decoder modularity.

Decoder	Err (°)	Infer (ms)	FLOPs (M)
Double	3.32	5.865	138.68
Single	7.18	5.739	138.92

Table 5: Ablation of decoder architecture. Comparison between dual region-specific GRUs and a single shared decoder.

Results in Table 5 show that the dual-decoder model achieves much higher accuracy (3.32° vs. 7.18°). This confirms the importance of disentangling temporal dynamics: one GRU specializes in rapid, fine-grained eye movements, while the other captures slower head-related variations. Collapsing both into a single decoder conflates these

signals, leading to entangled representations and reduced generalization.

In terms of efficiency, the single-decoder variant offers no meaningful advantage. Its inference time decreases only marginally (5.739 ms vs. 5.865 ms), while FLOPs slightly increase. Thus, the large performance drop cannot be justified by computational savings. Overall, the ablation demonstrates that region-specific decoders are essential for accurate gaze estimation.

We further investigated whether the benefits of dual decoders arise from parameter duplication or from region-specific specialization. Table 6 compares the standard configuration with two independent GRU decoders against a variant in which both decoders share weights while still processing their respective capsule streams.

Weight Sharing	Err (°)	Infer (ms)	FLOPs (M)
No	3.32	5.865	138.68
Yes	6.41	5.972	138.92

Table 6: Effect of weight sharing in dual decoders. Independent parameters enable specialization across facial regions.

The independent-weight model achieves 3.32° error, while enforcing weight sharing nearly doubles the error to 6.41° . Computational demands remain unchanged, with inference time and FLOPs showing negligible differences.

Taken together with the single-decoder ablation (Table 5), these results establish two clear design guidelines: (i) region-specific temporal streams are essential for precise gaze estimation, and (ii) parameter independence is necessary for these streams to realize their full potential. Importantly, this independence introduces virtually no computational overhead, yet reduces error by almost 50%, making it a practical and robust architectural choice.

With a single frame, the model frequently misclassifies left versus right gaze, particularly when head and eye directions diverge. Lacking motion cues, it essentially guesses horizontal orientation, leading to high error rates. In contrast, a nine-frame sequence provides temporal dynamics such as saccades and head rotations, which disambiguate symmetrical eye patterns.

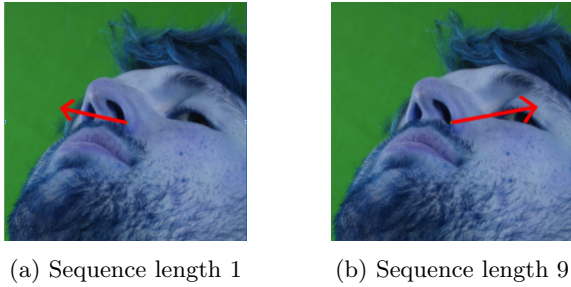


Fig. 3: Effect of temporal context. Single-frame prediction (left) often confuses left/right directions due to symmetrical appearances. A 9-frame sequence (right) leverages motion cues to resolve ambiguity.

From a system perspective, temporal modeling offers clear advantages. While single-frame approaches may suffice for coarse region detection, precise gaze direction requires multi-frame sequences. In our experiments, nine frames strike an effective balance: they provide enough temporal context to ensure accuracy while avoiding excessive latency.

Figure 4 illustrates how capsules learn to specialize in distinct facial regions on the ETH-XGaze validation set. The heatmaps show consistent localization of semantically meaningful areas, such as periocular regions, eyebrows, and the nose bridge, emerging without explicit supervision. This structured representation allows the decoders to weight region-relevant capsules (e.g., the eye decoder emphasizing eye-focused capsules) to produce accurate gaze predictions, closely aligned with the ground truth in rows 1 and 3.

The second row highlights a challenging case with partial occlusion from glasses. Here, eye-centric capsules are disrupted, yet the model maintains robust predictions by leveraging complementary cues from other capsules, such as head pose. The resulting error remains small ($\approx 2^\circ - 3^\circ$), demonstrating that hierarchical routing enables effective redundancy across facial regions.

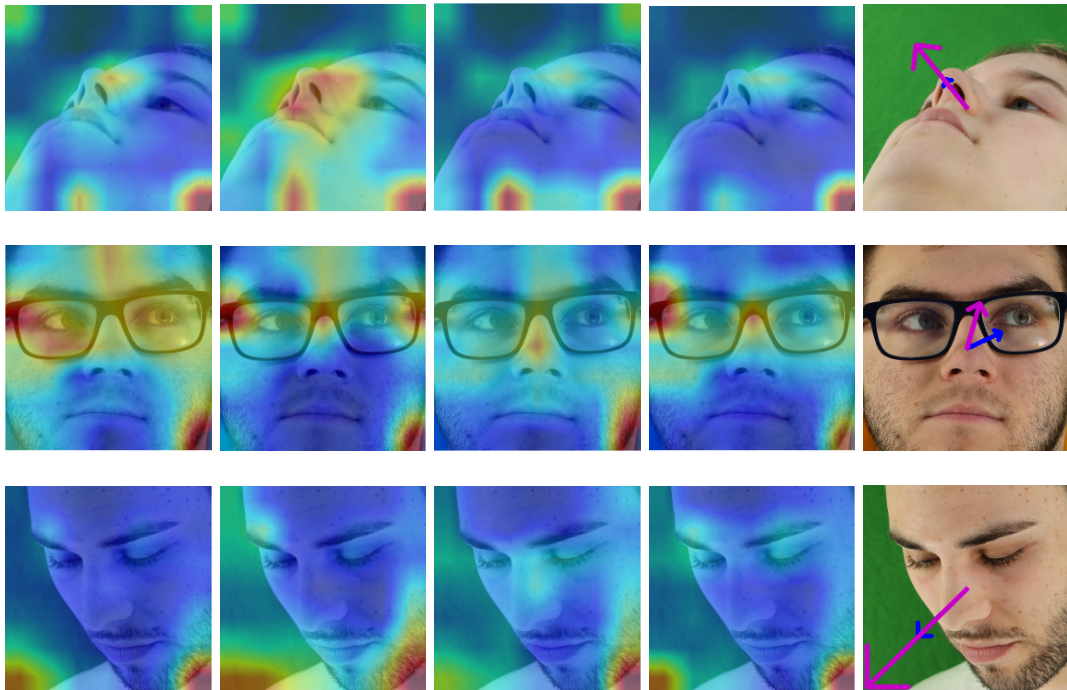


Fig. 4: Learned capsule attention and gaze prediction. Each row shows: (1-4) capsule heatmaps highlighting specialized regions, and (5) predicted (purple) vs. ground truth (blue) gaze.

Method	ETH-XGaze	MPIIFaceGaze	Gaze360	RTGene	Model Size
FullFace	7.38°	4.93°	14.99°	¹ 0°	196M
Gaze360	4.46°	4.06°	11.04°	7.08°	11.9M
SwAT	4.4°	5.00°	11.60°	N/A	26M
GazeTR-Hybrid	N/A	4.00°	10.62°	6.55°	0.0
L2CS-Net	N/A	3.92°	10.41°	N/A	11.9M
GazeNeRF	6.94°	14.93°	N/A	N/A	18M
PoolFormer	3.67°	N/A	N/A	N/A	56M
GazeCaps	N/A	4.06°	10.04°	6.92°	11.7M
GazeCapsNet	5.75°	4.06°	5.10°	N/A	11.7M
Ours	3.36°	2.65°	9.06°	4.76°	13.00M

Table 7: Cross-dataset benchmarking. Angular error (°) of different gaze estimation methods on ETH-XGaze, MPIIFaceGaze, Gaze360, and RT-GENE, along with model size.

5.3 Performance Evaluation

We benchmarked the proposed architecture against state-of-the-art methods on four representative datasets covering complementary challenges in gaze estimation. ETH-XGaze, with over one million images and head poses spanning $\pm 90^\circ$, tests robustness under extreme orientations (Zhang et al., 2020). MPIIFaceGaze, containing more than 200,000 webcam frames, assess subject-specific variability in unconstrained daily conditions (Zhang et al., 2015). Gaze360, with 172,000 frames covering full 360° viewpoints, evaluates performance under spherical and in-the-wild settings (Kellnhofer et al., 2019). Finally, RT-GENE, with around 120,000 stereo images, provides a benchmark for real-time human-robot interaction scenarios (Fischer, Chang, & Demiris, 2018b). Together, these datasets encompass critical dimensions of the task, including extreme poses, inter-subject generalization, unconstrained environments, and temporal stability.

Quantitative results in Table 7 show that our model consistently achieves state-of-the-art accuracy while maintaining compact size and real-time performance.

On ETH-XGaze, our model achieves a new benchmark of 3.36° , a 19% improvement over prior work. On MPIIFaceGaze, it reaches 2.65° , highlighting strong adaptability to inter-subject variability without calibration. On Gaze360, it maintains competitive accuracy (9.06°), though 3D-aware approaches like GazeCapsNet achieve lower error at higher computational cost. Finally, on RT-GENE, it delivers 4.76° while preserving

stable predictions during rapid head movements and occlusions, essential for social robotics.

Compared to GazeCapsNet, the trade-offs are clear. Its explicit 3D modeling yields advantages for full spherical coverage, but at greater computational cost (20 ms vs. our 8.2 ms) and with more demanding supervision. Our method offers superior performance on ETH-XGaze and MPIIFaceGaze with simpler training requirements, making it more practical for real-time interactive systems.

Figure 5 provides qualitative evidence of these behaviors. On ETH-XGaze (a-d), the model preserves accuracy even at extreme $\pm 90^\circ$ yaw angles where conventional CNNs fail. On MPIIFaceGaze (e-h), it adapts to differences in eyelid shape and facial structure without explicit calibration. On Gaze360 (i-l), it produces stable predictions under challenging real-world conditions such as variable lighting and partial occlusions. Finally, on RT-GENE (m-p), it remains consistent during natural head motion and transient occlusions, supporting its suitability for human-robot interaction.

6 Discussion

The experimental results presented in this work highlight several key insights into the design of efficient and accurate gaze estimation systems.

The ablation studies also confirm the necessity of modularity in our architecture. Capsules provide structured, region-specific representations of facial features, while self-attention mechanisms refine the contributions dynamically. The

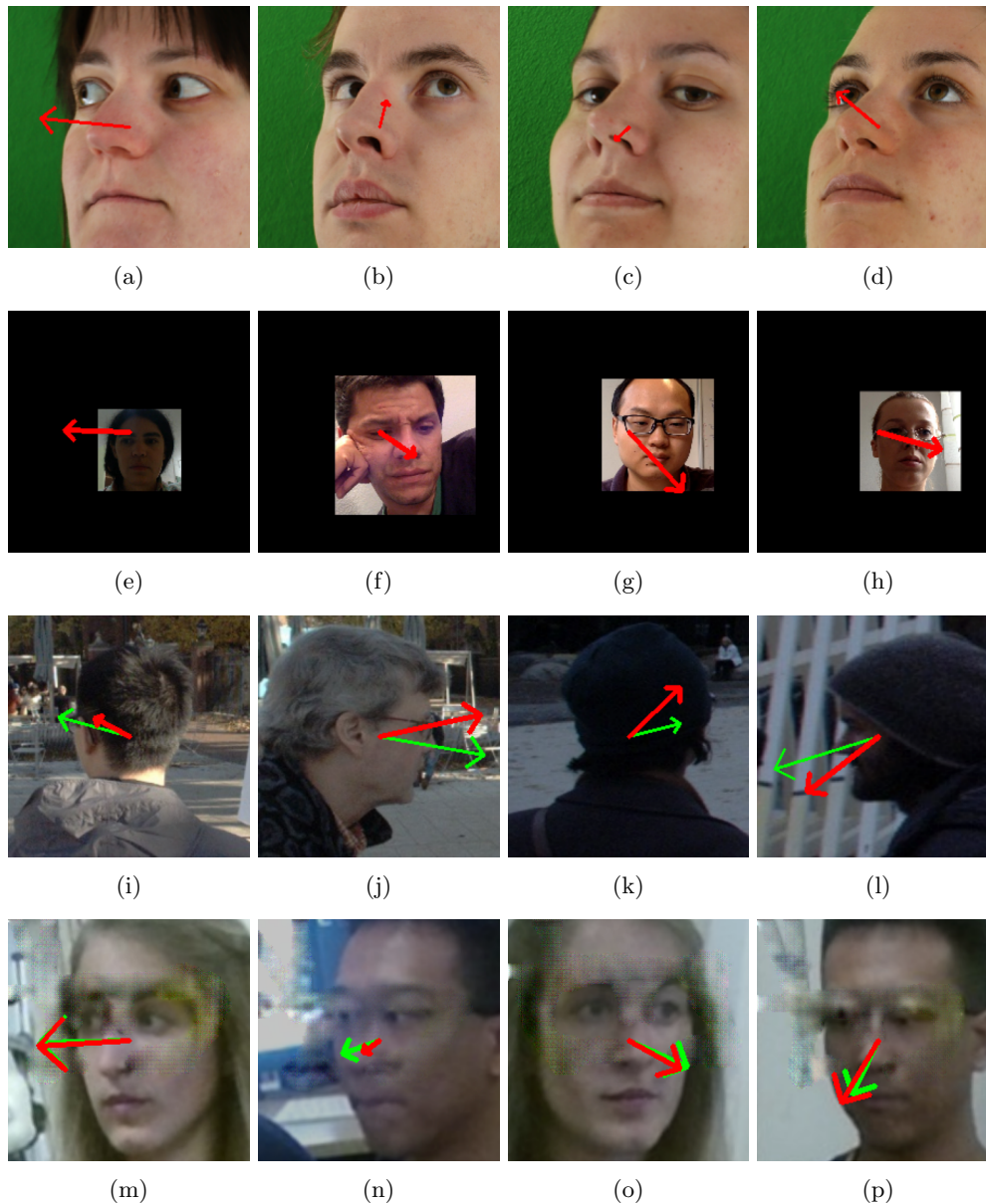


Fig. 5: Qualitative results across datasets. (a-d) ETH-XGaze: robustness to extreme head poses. (e-h) MPIIFaceGaze: adaptability to inter-subject variability. (i-l) Gaze360: resilience in unconstrained conditions (lighting, occlusion). (m-p) RT-GENE: stability in human-robot interaction scenarios.

dual GRU decoders further disentangle temporal dynamics by allowing independent specialization: one pathway captures rapid eye movements, while the other models slower head-pose variations. Importantly, experiments with decoder

weight sharing demonstrated that parameter independence is essential for maintaining this specialization, as performance degraded substantially when both streams were forced to share weights. Together, these results validate the principle that

modularity and specialization yield more expressive and robust representations than monolithic or parameter-shared designs.

Another consistent observation is that gaze estimation is inherently a spatiotemporal problem. Our comparison between single-frame and multi-frame inputs revealed that temporal context is indispensable for resolving ambiguities, such as left-right confusion, which cannot be disambiguated from static spatial features alone. The nine-frame configuration adopted here provided sufficient temporal cues to achieve robust accuracy without introducing significant latency, mirroring the short-term integration window often required for human visual interpretation. This confirms that practical gaze estimation solutions must jointly exploit both spatial and temporal information.

Beyond quantitative performance, our architecture also demonstrates strong interpretability and resilience. Capsule visualizations reveal consistent specialization toward semantically meaningful regions, such as periocular areas, eyebrows, or the nose bridge. This property not only provides a degree of transparency for error analysis but also contributes to robustness. For example, when eye regions are occluded by glasses, the model compensates by relying on head-pose cues captured by other capsules, resulting in only minor accuracy degradation. This redundancy across spatially organized parts reduces reliance on any single feature source, enhancing robustness under naturalistic conditions.

A central theme across our evaluations is the balance between accuracy and efficiency. While larger architectural configurations, such as increasing capsule count or dimensionality, slightly increase representational capacity, they yield negligible performance gains and often introduce redundancy. By contrast, the proposed configuration with four capsules, four attention heads, and moderate GRU hidden dimensions consistently achieved the best trade-off, delivering high accuracy with compact size and real-time inference. These findings underscore the importance of designing lean architectures that avoid unnecessary complexity, particularly for deployment in interactive applications where low latency is critical.

Cross-dataset benchmarking further reinforces these conclusions. On ETH-XGaze and MPI-IFaceGaze, our model establishes new state-of-the-art results, demonstrating both its accuracy and adaptability to inter-subject variability without the need for subject-specific calibration. On Gaze360, performance remains competitive, though specialized 3D-aware methods such as GazeCapsNet achieve superior results in extreme pose scenarios. Nevertheless, our method achieves these results at substantially lower computational cost, with faster inference and only 2D supervision requirements. Finally, in RT-GENE, the architecture proves robust in real-world interaction settings, maintaining stable predictions despite rapid head movements and intermittent occlusions; conditions especially suited for social robotics applications.

These comparisons highlight the trade-offs inherent in different architectural paradigms. Transformer-based models underperformed in our experiments, likely due to their weaker spatial coherence, whereas CNN-based backbones such as ConvNeXt proved better aligned with the spatial priors of the gaze estimation task. Capsule-based approaches like GazeCapsNet excel at 3D spherical estimation but require greater computational resources and more complex annotations. Our design therefore occupies a complementary position: more efficient and practical for real-time human-robot interaction and assistive technologies, while still competitive accuracy across diverse benchmarks.

To further demonstrate the applicability of our method, we provide a supplementary video showcasing three real-time scenarios. These illustrate the robustness of the model in challenging head poses, its stability under dynamic movements, and its adaptability in human-robot interaction contexts. The video highlights that the proposed approach not only achieves state-of-the-art accuracy in benchmark datasets, but also operates seamlessly in practical conditions where low latency is crucial.

In summary, the proposed architecture demonstrates that combining modular capsule representations, attention-based routing, and region-specific temporal decoders yields an effective balance of accuracy, efficiency, and interpretability. The model’s robustness across datasets and conditions suggests strong potential for real-world

applications in interactive systems, where gaze estimation serves as a key enabler of natural and reliable human-machine engagement.

7 Conclusions and Future Work

This work has presented an architecture for gaze estimation that integrates separate processing pathways for eye movements and head dynamics, resulting in notable improvements in accuracy, stability, and temporal consistency. The combination of capsule-based spatial reasoning with frozen convolutional feature extraction enables both interpretability and efficiency, reaching state-of-the-art accuracy (3.36° error on ETH-XGaze) while maintaining real-time operation (8.23 ms/frame). These advances open promising perspectives for human-centered applications, from natural interaction in social robotics to personalized assistive technologies. At the same time, the current design still faces challenges. Compared to prior gaze estimation models, our approach already alleviates several known bottlenecks: reliance on 2D supervision is mitigated by improved robustness to head pose variation, temporal modeling is enhanced by explicitly integrating dynamic pathways, and the efficiency of our architecture allows real-time operation on modern GPUs. Nevertheless, these aspects remain only partially resolved. Performance still degrades in extreme head poses where annotated data is scarce, temporal reasoning is constrained by the use of fixed-length sequences, and computational demand can pose difficulties for deployment on low-power edge devices. These considerations underline that, while our framework advances the state of the art, it also highlights open opportunities for continued refinement.

Building on these findings, several future research avenues emerge to further enhance both biological fidelity and technical performance. Immediate extensions include incorporating optical flow to better capture motion dynamics, and deploying the model on robotic platforms for active 3D gaze target localization in interactive environments. At the architectural level, enhancements such as dynamic capsule dimensionality, landmark-guided capsule initialization, and attention-gated feature modulation could improve

anatomical grounding, while expansions toward body pose integration would enable modeling of eye-head-body coordination. Temporal processing may benefit from predictive coding, multi-scale recurrent modeling, and memory-augmented attention mechanisms to capture longer-term dependencies. On the learning side, self-supervised and meta-learning strategies could reduce reliance on annotated data and enable few-shot personalization, while developmental and reinforcement learning paradigms offer avenues to mimic natural gaze acquisition and adaptation. Together, these directions highlight the potential of interdisciplinary approaches that merge neuroscience and artificial intelligence, charting a path toward more robust, adaptive, and human-like gaze estimation systems deployable in both standalone and embodied robotic applications.

Acknowledgements. We would like to thank Maria Vanrell Martorell (UAB) for her valuable guidance and support during the development of this article. Part of this research was conducted as part of the author’s Master’s dissertation in Computer Vision.

Declarations

- **Funding:** This work is partially funded by the Spanish Ministry of Science and Innovation under project PID2021-122402OB-C22 and by the Basque Government under project IT1427-22.
- **Conflict of interest/Competing interests** (check journal-specific guidelines for which heading to use): The authors have no relevant financial or non financial Conflict of Interest to declare.
- **Ethics approval and consent to participate:** Informed consent was obtained from all individual participants included in the study.
- **Consent for publication:** The authors affirm that all human persons provided informed consent for publications of the images.
- **Code availability:** Related code is available at <https://github.com/toukapy/capsStare>
- **Author contribution:** All authors contributed equally to the work.

References

- Abdelrahman, A.A., Hempel, T., Khalifa, A., Al-Hamadi, A., Dinges, L. (2023). L2cs-net : Fine-grained gaze estimation in unconstrained environments. *2023 8th international conference on frontiers of signal processing (icfsp)* (p. 98-102). (<https://doi.org/10.1109/ICFSP59764.2023.10372944>)
- Admoni, H., & Scassellati, B. (2017, 03). Social eye gaze in human-robot interaction: A review. *Journal of Human-Robot Interaction*, 6, 25, <https://doi.org/10.5898/JHRI.6.1.Admoni>
- Brooks, R., & Meltzoff, A. (2005, 12). The development of gaze following and its relation to language. *Developmental science*, 8, 535-43, <https://doi.org/10.1111/j.1467-7687.2005.00445.x>
- Byers-Heinlein, K., Tsui, R.K., van Renswoude, D., Black, A.K. (2021). The development of gaze following in monolingual and bilingual infants: A multi-laboratory study. *Infancy*, 26(1), 4-38, <https://doi.org/10.1111/infa.12360> Retrieved from <https://doi.org/10.1111/infa.12360>
- Cheng, Y., & Lu, F. (2022). Gaze estimation using transformer. *2022 26th international conference on pattern recognition (icpr)* (p. 3341-3347).
- Cho, K., van Merriënboer, B., Gulcehre, C., Bahdanau, D., Bougares, F., Schwenk, H., Bengio, Y. (2014, October). Learning phrase representations using RNN encoder-decoder for statistical machine translation. A. Moschitti, B. Pang, & W. Daelemans (Eds.), *Proceedings of the 2014 conference on empirical methods in natural language processing (EMNLP)* (pp. 1724-1734). Doha, Qatar: Association for Computational Linguistics. Retrieved from <https://aclanthology.org/D14-1179/>
- Deber, J., Jota, R., Forlines, C., Wigdor, D. (2015). How much faster is fast enough? user perception of latency & latency improvements in direct and indirect touch. *Proceedings of the 33rd annual acm conference on human factors in computing systems* (pp. 1827-1836).
- Duchowski, A.T. (2017). *Eye tracking methodology: Theory and practice* (3rd ed.). Cham: Springer.
- D'Amelio, A., Cartella, G., Cuculo, V., Lucchi, M., Cornia, M., Cucchiara, R., Boccignone, G. (2025). Tpp-gaze: Modelling gaze dynamics in space and time with neural temporal point processes. *2025 ieee/cvf winter conference on applications of computer vision (wacv)* (p. 8786-8795).
- Emery, N.J. (2000). The eyes have it: the neuroethology, function and evolution of social gaze. *Neuroscience & Biobehavioral Reviews*, 24(6), 581-604,
- Ewaisha, M., El Shwarby, M., Abbas, H., Sobh, I. (2020). End-to-end multitask learning for driver gaze and head pose estimation. *Electronic Imaging*, 32, 1-6,
- Farkhondeh, A., Palmero, C., Scardapane, S., Escalera, S. (2022). Towards self-supervised gaze estimation.. (Publisher Copyright: © 2022. The copyright of this document resides with its authors. It may be distributed unchanged freely in print or electronic forms.; 33rd British Machine Vision Conference Proceedings, BMVC 2022 ; Conference date: 21-11-2022 Through 24-11-2022)
- Fischer, T., Chang, H., Demiris, Y. (2018b, October 7). Rt-gene: Real-time eye gaze estimation in natural environments. V. Ferrari, M. Hebert, C. Sminchisescu, & Y. Weiss (Eds.), *Computer vision - eccv 2018* (1st ed., pp. 339-357). Springer. (The European Conference on Computer Vision (ECCV), 2018 ; Conference date: 08-09-2018 Through 14-09-2018)

- Fischer, T., Chang, H.J., Demiris, Y. (2018a). RT-GENE: Real-time eye gaze estimation in natural environments. *European conference on computer vision (eccv)* (pp. 334–352).
- Franchak, J.M., & Yu, C. (2022). Beyond screen time: Using head-mounted eye tracking to study natural behavior. *Advances in Child Development and Behavior*, 62, 61–91, <https://doi.org/10.1016/bs.acdb.2021.11.001> Retrieved from <https://doi.org/10.1016/bs.acdb.2021.11.001>
- He, K., Zhang, X., Ren, S., Sun, J. (2016). Deep residual learning for image recognition. *2016 IEEE conference on computer vision and pattern recognition (cvpr)* (p. 770–778).
- Jindal, S., Yadav, M., Manduchi, R. (2024a). Spatio-temporal attention and gaussian processes for personalized video gaze estimation. *Proceedings of the IEEE/CVF conference on computer vision and pattern recognition* (pp. 604–614).
- Jindal, S., Yadav, M., Manduchi, R. (2024b, June). Spatio-Temporal Attention and Gaussian Processes for Personalized Video Gaze Estimation. *2024 IEEE/CVF conference on computer vision and pattern recognition workshops (cvprw)* (p. 604–614). Los Alamitos, CA, USA: IEEE Computer Society. (<https://doi.ieeecomputersociety.org/10.1109/CVPRW63382.2024.00065>)
- Kellnhofer, P., Recasens, A., Stent, S., Matusik, W., Torralba, A. (2019, October). Gaze360: Physically unconstrained gaze estimation in the wild. *IEEE international conference on computer vision (iccv)*.
- Krafka, K., Khosla, A., Kellnhofer, P., Kannan, H., Bhandarkar, S., Matusik, W., Torralba, A. (2016, June). Eye Tracking for Everyone. *2016 IEEE conference on computer vision and pattern recognition (cvpr)* (p. 2176–2184). Los Alamitos, CA, USA: IEEE Computer Society. (<https://doi.ieeecomputersociety.org/10.1109/CVPR.2016.239>)
- Krizhevsky, A., Sutskever, I., Hinton, G. (2012, 01). Imagenet classification with deep convolutional neural networks. *Neural Information Processing Systems*, 25, , <https://doi.org/10.1145/3065386>
- Kuang, C., O. Kephart, J., Ji, Q. (2024, 16 Dec). Interaction-aware dynamic 3D gaze estimation in videos. A. Madu Blessing, J. Wu, D. Zanca, E. Krupinski, S. Kashyap, & A. Karargyris (Eds.), *Proceedings of the 2nd gaze meets ml workshop* (Vol. 226, pp. 107–124). PMLR.
- Lai, B., Liu, M., Ryan, F., et al. (2024). In the eye of transformer: Global–local correlation for egocentric gaze estimation and beyond. *International Journal of Computer Vision*, 132, 854–871, (<https://doi.org/10.1007/s11263-023-01879-7>)
- Liu, Z., Mao, H., Wu, C.-Y., Feichtenhofer, C., Darrell, T., Xie, S. (2022). A convnet for the 2020s. *2022 IEEE/CVF conference on computer vision and pattern recognition (cvpr)* (p. 11966–11976).
- Nonaka, S., Nobuhara, S., Nishino, K. (2022, June). Dynamic 3D Gaze from Afar: Deep Gaze Estimation from Temporal Eye-Head-Body Coordination. *2022 IEEE/CVF conference on computer vision and pattern recognition (cvpr)* (p. 2182–2191). Los Alamitos, CA, USA: IEEE Computer Society. (<https://doi.ieeecomputersociety.org/10.1109/CVPR52688.2022.00223>)
- Oishi, S., Koide, K., Yokozuka, M., Banno, A. (2021). 4d attention: Comprehensive framework for spatio-temporal gaze mapping. *IEEE Robotics and Automation Letters*, 6(4), 7240–7247,
- Palinko, O., Sciutti, A., Rea, F. (2022). Gaze-based intention estimation for shared autonomy in assembly tasks. *IEEE/rsj international conference on intelligent robots and systems (iros)* (p. 11342–11349).

- Palmero Cantarino, C., Komogortsev, O.V., Talathi, S.S. (2020, June). Benefits of temporal information for appearance-based gaze estimation. *Acm symposium on eye tracking research and applications* (p. 1–5). ACM. Retrieved from <http://dx.doi.org/10.1145/3379156.3391376>
- Pijpaert, A.R., Goossens, H., van Dijk, B.W., Roetman, L., van Nispen, R.M., van Rijn, L.J. (2025). A validation study on the accuracy and precision of gaze and vergence using stereoscopic eye-tracking technology. *Behavior Research Methods*, 57(8), 214,
- Ruzzi, A., Shi, X., Wang, X., Li, G., De Mello, S., Chang, H.J., ... Hilliges, O. (2023). Gazenerf: 3d-aware gaze redirection with neural radiance fields. *2023 ieee/cvf conference on computer vision and pattern recognition (cvpr)* (p. 9676-9685).
- Sabour, S., Frosst, N., Hinton, G.E. (2017). Dynamic routing between capsules. *Advances in Neural Information Processing Systems (NeurIPS)*, 30, ,
- Simonyan, K., & Zisserman, A. (2015). Very deep convolutional networks for large-scale image recognition. *3rd international conference on learning representations (iclr 2015)* (pp. 1–14).
- Singh, V., Langde, C., Lakotia, S., Kannan, V., Ahmed, S. (2024). Eg-sif: Improving appearance based gaze estimation using self improving features. *Gaze meets machine learning workshop* (pp. 219–235).
- Stappen, L., Rizos, G., Schuller, B. (2020). X-aware: Context-aware human-environment attention fusion for driver gaze prediction in the wild. *Proceedings of the 2020 international conference on multimodal interaction* (pp. 858–867).
- Stower, R., Kappas, A., Hoffman, G., Leite, I. (2021). A meta-analysis of children’s trust in social robots. *International Journal of Social Robotics*, 13, 1979–2001, <https://doi.org/10.1007/s12369-021-00789-3>
- Vaswani, A., Shazeer, N., Parmar, N., Uszkoreit, J., Jones, L., Gomez, A.N., ... Polosukhin, I. (2017). Attention is all you need. *Proceedings of the 31st international conference on neural information processing systems* (p. 6000–6010). Red Hook, NY, USA: Curran Associates Inc.
- Wang, H., Oh, J., Chang, H., Na, J., Tae, M., Zhang, Z., Choi, S.-I. (2023, 06). GazeCaps: Gaze estimation with self-attention-routed capsules. (p. 2669-2677).
- Yan, C., Pan, W., Xu, C., Dai, S., Li, X. (2023). Gaze estimation via strip pooling and multi-criss-cross attention networks. *Applied Sciences*, 13(10), , <https://doi.org/10.3390/app13105901> Retrieved from <https://www.mdpi.com/2076-3417/13/10/5901>
- Zhang, X., Park, S., Beeler, T., Bradley, D., Tang, S., Hilliges, O. (2020). Eth-xgaze: A large scale dataset for gaze estimation under extreme head pose and gaze variation. *Computer vision – eccv 2020: 16th european conference, glasgow, uk, august 23–28, 2020, proceedings, part v* (p. 365–381). Berlin, Heidelberg: Springer-Verlag.
- Zhang, X., Sugano, Y., Bulling, A. (2019). Evaluation of appearance-based methods and implications for gaze-based applications. *Proceedings of the 2019 chi conference on human factors in computing systems* (p. 1–13). New York, NY, USA: Association for Computing Machinery. Retrieved from <https://doi.org/10.1145/3290605.3300646>
- Zhang, X., Sugano, Y., Fritz, M., Bulling, A. (2015, June). Appearance-based gaze estimation in the wild. *2015 ieee conference on computer vision and pattern recognition (cvpr)* (p. 4511–4520). IEEE. Retrieved from <http://dx.doi.org/10.1109/CVPR.2015.7299081>

Zhang, X., Sugano, Y., Fritz, M., Bulling, A. (2017, July). It's written all over your face: Full-face appearance-based gaze estimation. *2017 IEEE Conference on Computer Vision and Pattern Recognition Workshops (CVPRW)*. IEEE. Retrieved from <http://dx.doi.org/10.1109/CVPRW.2017.284>